Tuberculous Granuloma Induction via Interaction of a Bacterial Secreted Protein with Host Epithelium

Hannah E. Volkman, *et al.*

Science **327**, 466 (2010);
DOI: 10.1126/science.1179663

27. M. C. Harrisingh, Y. Wu, G. A. Lnenicka, M. N. Nitabach, *J. Neurosci.* **27**, 12489 (2007).

28. We thank P. Nakatani (Dana-Farber Cancer Institute) for the FH cassette; P. Sassone-Corsi (University of California, Irvine) for BMAL1 antiserum; M. J. Weber (University of Virginia), D. Mochly-Rosen (Stanford University), P. Blumberg (National Cancer Institute), and M. Grossi (University of Rome), respectively, for RACK1, C2, PKCα, and MYOD cDNAs; M. Liu for expert technical assistance; N. Vujovic for help with transactivation assays; and L. Lande-Diner for comments on the manuscript. Supported by grants from the Edward R. and Anne G. Lefler Center and the G. Harold and Leila Y. Mathers Charitable Foundation (C.J.W.), an Edward R. and Anne G. Lefler Center postdoctoral fellowship (M.S.R.), a Swiss National Science Foundation grant (D.K.), and an EMBO postdoctoral fellowship (C.B.).

Supporting Online Material
www.sciencemag.org/cgi/content/full/327/5964/463/DC1
Materials and Methods
SOM Text
Figs. S1 to S6
References

3 August 2009; accepted 7 December 2009
10.1126/science.1180067

Tuberculous Granuloma Induction via Interaction of a Bacterial Secreted Protein with Host Epithelium

Hannah E. Volkman,[1]* Tamara C. Pozos,[2]*† John Zheng,[2] J. Muse Davis,[3] John F. Rawls,[4,5] Lalita Ramakrishnan[6,7,8]‡

Granulomas, organized aggregates of immune cells, are a hallmark of tuberculosis and have traditionally been thought to restrict mycobacterial growth. However, analysis of *Mycobacterium marinum* in zebrafish has shown that the early granuloma facilitates mycobacterial growth; uninfected macrophages are recruited to the granuloma where they are productively infected by *M. marinum*. Here, we identified the molecular mechanism by which mycobacteria induce granulomas: The bacterial secreted protein 6-kD early secreted antigenic target (ESAT-6), which has long been implicated in virulence, induced matrix metalloproteinase–9 (MMP9) in epithelial cells neighboring infected macrophages. MMP9 enhanced recruitment of macrophages, which contributed to nascent granuloma maturation and bacterial growth. Disruption of MMP9 function attenuated granuloma formation and bacterial growth. Thus, interception of epithelial MMP9 production could hold promise as a host-targeting tuberculosis therapy.

Tuberculous infection begins with recruitment of monocytes to a peripheral infection site where they engulf mycobacteria and migrate to deeper tissues (*1*, *2*). Additional macrophages and other immune cells then aggregate with the infected cells to form granulomas (*3*). Granulomas, recognized as pathological hallmarks of tuberculosis for over a century, were thought to curtail infection by encasing mycobacteria (*4*). However, visualization of granuloma formation in transparent zebrafish larvae infected with *Mycobacterium marinum* (Mm) has revealed that the early granuloma serves to expand bacterial numbers (*5*, *6*). An infected macrophage induces granuloma formation by promoting recruitment of additional phagocytes (*6*). Upon its death, multiple newly arriving macrophages phagocytose it and thereby become infected. Concerted iteration of these processes makes the early granuloma a site for bacterial expansion (*6*). Mycobacteria direct these granuloma-forming processes via their region of difference–1 (RD1) virulence locus that encodes the ESAT-6 secretion system–1 (ESX-1) secretion system (*5*, *6*). The host factors coopted in RD1-mediated granuloma formation remain unknown.

In a host gene expression survey comparing zebrafish larvae infected with wild-type Mm (WT) or RD1-deleted Mm (ΔRD1) (*5*, *6*), we identified *matrix metalloproteinase 9* (*mmp9*) and *tissue inhibitor of metalloproteinase 2b* (*timp2b*) as being RD1-induced during granuloma formation at 5 days post infection (5 dpi) (Fig. 1, A and B; tables S1 to 4; and fig. S1, A and B). To control for ΔRD1's attenuated infection at 5 dpi (*5*), we confirmed RD1-dependent gene induction using higher ΔRD1 inoculations that produced similar bacterial burdens at 5 dpi with the expected paucity of ΔRD1 granulomas (*5*, *6*) (Fig. 1, A and C, and fig. S1C). At 1 dpi, only *mmp9* was induced, suggesting that *timp2b* induction at 5 dpi was a compensatory response to increased *mmp9* (Fig. 1D). Mmp9 is a gelatinase, and gelatin zymography confirmed that RD1-dependent *mmp9* mRNA expression resulted in increased Mmp9 gelatinase activity (Fig. 1E). In contrast, mRNA expression and activity of another gelatinase Mmp2 were not altered by infection (fig. S1A and Fig. 1E).

MMP9 is implicated in the pathogenesis of several inflammatory conditions (*7*, *8*) and is highly expressed in human tuberculosis as well as in the mouse model of tuberculosis (*9*–*12*) (table S1). In mice, MMP9 activity correlates to increased macrophage migration and granuloma formation; however, it is reported to be a host resistance factor, perhaps because its expression is associated with variable effects on infection in different genetic backgrounds (*10*). In humans, MMP9 clearly mediates susceptibility as its increased activity is correlated with worse outcomes (*9*). To test *mmp9*'s role in promoting granuloma formation and virulence, we knocked down its expression transiently with three modified antisense oligonucleotides (morpholinos) (*1*, *13*) (fig. S2). The morpholinos, singly or in combination, reduced gelatinase activity reliably up to 4 dpi with activity returning to control levels by 5 dpi (fig. S2). WT infection of morpholino-injected embryos (morphants) resulted in attenuated infection sharing several features of ΔRD1 infection of control embryos. First, morphants displayed reduced numbers of bacteria and granulomas, as well as increased host survival (Fig. 2, A to C). Second, kinetic analyses of granuloma formation in the morphants confirmed a specific granuloma-forming deficit (Fig. 2, D to F). We found a dynamic link between Mmp9 activity, granuloma formation, and bacterial expansion: Bacterial burdens and granuloma formation differed only up to 4 dpi, returning to control levels by 5 dpi contemporaneous with restoration of Mmp9 activity (Fig. 2, A to E, and fig. S2). Finally, although the RD1 locus promotes macrophage recruitment to nascent granulomas, it is not required for initial phagocyte migration to infecting bacteria when they are still extracellular (*5*, *6*). Similarly, *mmp9* morphants displayed normal macrophage migration to extracellular bacteria when injected into the hindbrain ventricle (fig. S3).

RD1 probably contributes to granuloma expansion through pleiotropic effects that include inducing apoptosis of infected macrophages and recruiting new uninfected macrophages (*5*, *6*, *14*–*16*). In contrast, Mmp9 was not required for RD1-induced cell death; morphant and control granulomas in WT infection contained similar numbers of TUNEL (terminal deoxynucleotidyl transferase–mediated deoxyuridine triphosphate nick end labeling)–positive cells, whereas control granulomas in ΔRD1 infection exhibited the expected reduction (*13*) (Fig. 2G). Thus RD1-induced apoptosis is Mmp9 independent and cannot mediate bacterial ex-

[1]Molecular and Cellular Biology Graduate Program, University of Washington, Seattle, WA 98155, USA. [2]Department of Pediatrics, University of Washington, Seattle, WA 98155, USA. [3]Immunology and Molecular Pathogenesis Graduate Program, Emory University, Atlanta, GA 30322, USA. [4]Department of Cell and Molecular Physiology, University of North Carolina, Chapel Hill, NC 27599, USA. [5]Department of Microbiology and Immunology, University of North Carolina, Chapel Hill, NC 27599, USA. [6]Department of Microbiology, University of Washington, Seattle, WA 98155, USA. [7]Department of Medicine, University of Washington, Seattle, WA 98155, USA. [8]Department of Immunology, University of Washington, Seattle, WA 98155, USA.

*These authors contributed equally to this work.
†Present address: Pediatric Infectious Diseases and Immunology, Children's Hospitals and Clinics of Minnesota, St. Paul, MN 55102, USA.
‡To whom correspondence should be addressed. E-mail: lalitar@u.washington.edu

pansion in the absence of new macrophage recruitment, and Mmp9-mediated acceleration of macrophage recruitment to granulomas is an independent mediator of pathogenesis.

Multiple cell types express *MMP9* in many inflammatory conditions (*7*). In the context of tuberculosis, it is induced in cultured monocytes infected with *Mycobacterium tuberculosis* (*9*, *17*–*19*) and in epithelial cells (*20*). In advanced human tuberculosis, induced expression is reported in some monocytes and multinucleated giant cells abutting necrotic centers of

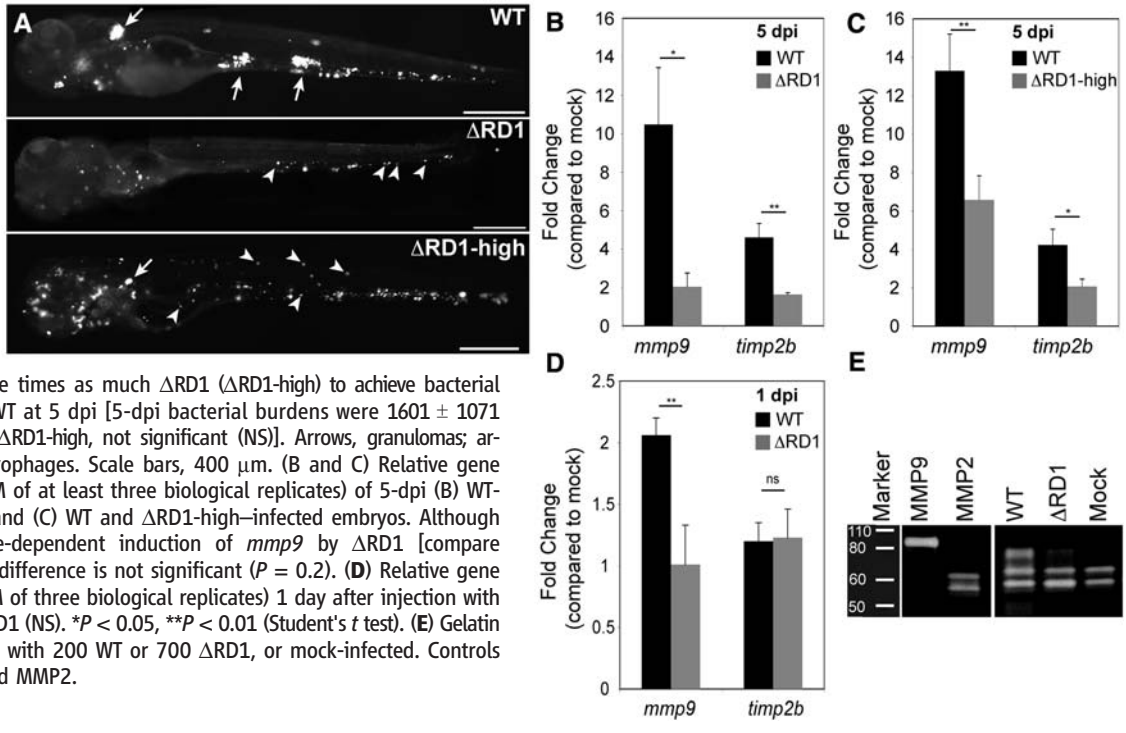

Fig. 1. RD1-dependent Mmp9 induction. (**A**) Representative fluorescence images of 5-dpi embryos used for gene expression studies in (**B** and **C**). Embryos in the top and middle panels were injected with similar doses of WT and ΔRD1, respectively (WT dose of 193 ± 36 and ΔRD1 dose of 217 ± 63), where ΔRD1 bacterial burdens are lower than those of WT at 5 dpi. Embryo in bottom panel was injected with ~ five times as much ΔRD1 (ΔRD1-high) to achieve bacterial burdens similar to those of WT at 5 dpi [5-dpi bacterial burdens were 1601 ± 1071 for WT and 1531 ± 1011 for ΔRD1-high, not significant (NS)]. Arrows, granulomas; arrowheads, single infected macrophages. Scale bars, 400 μm. (B and C) Relative gene expression levels (mean ± SEM of at least three biological replicates) of 5-dpi (B) WT- and ΔRD1-infected embryos and (C) WT and ΔRD1-high–infected embryos. Although there appears to be a dose-dependent induction of *mmp9* by ΔRD1 [compare induction in (B) and (C)], the difference is not significant ($P = 0.2$). (**D**) Relative gene expression levels (mean ± SEM of three biological replicates) 1 day after injection with 721 ± 39 WT or 484 ± 147 ΔRD1 (NS). *$P < 0.05$, **$P < 0.01$ (Student's *t* test). (**E**) Gelatin zymography of embryos 5 dpi with 200 WT or 700 ΔRD1, or mock-infected. Controls are purified human MMP9 and MMP2.

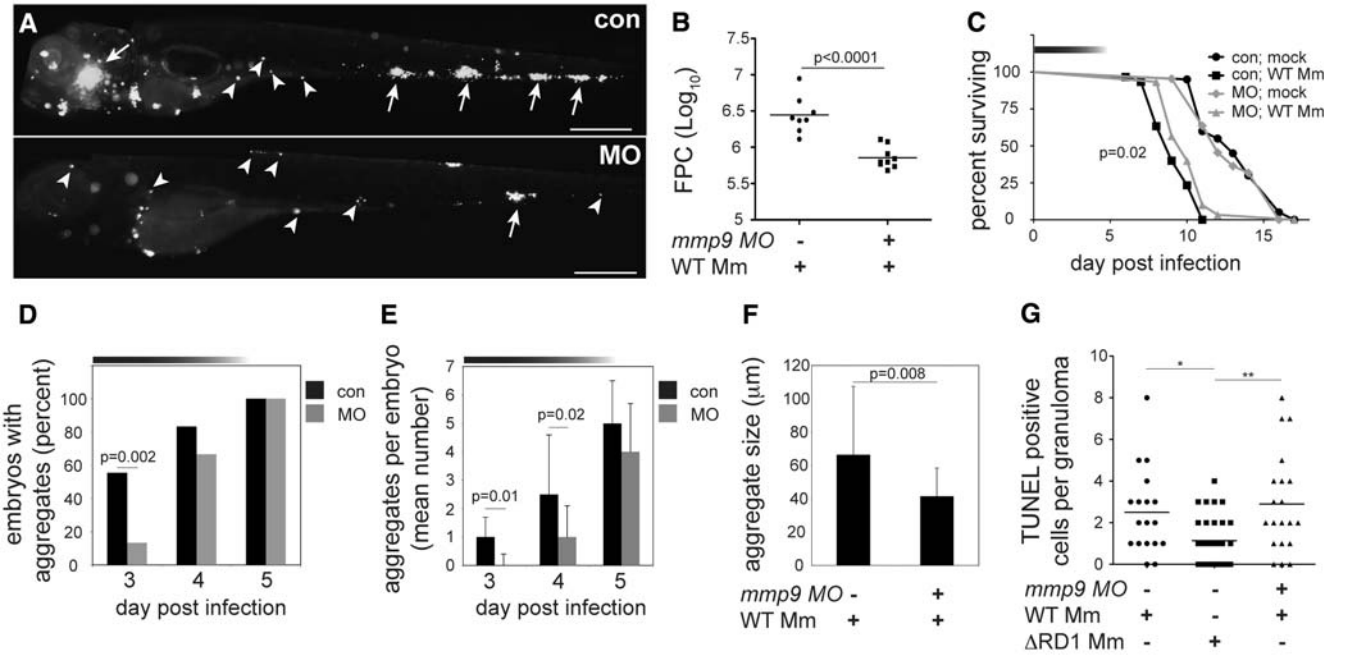

Fig. 2. Mmp9 promotes granuloma formation and virulence. (**A**) Fluorescence images of representative control (con) and *mmp9* morphant (MO) embryos 4 dpi with 116 WT. Arrows, granulomas; arrowheads, single infected macrophages. Scale bars, 400 μm. (**B**) Bacterial burdens of all 4-dpi embryos determined by fluorescence pixel counts (FPC) (*31*). (**C**) Survival of con and MO embryos ($n = 30$ each) infected with 150 colony-forming units (CFU) of WT or mock-infected ($n = 20$ each). Median survival was 10 days for infected MO and 9 days for infected con ($P = 0.02$; log-rank test) and no different for uninfected MO and con. Top horizontal bar denotes duration of MO activity (fig. S2). (**D** to **F**) Kinetics of granuloma formation in con and MO embryos infected with 101 WT. Data in (D) were analyzed by Fisher's exact test of a contingency table. Bars in (E) and (F) represent the mean ± SEM (Student's *t* test). (**G**) Median number of TUNEL-positive cells per con or MO granuloma 4 dpi with 37 CFU of WT and con granulomas 4 dpi with 585 ΔRD1 (one-way analysis of variance; $P = 0.003$, with Dunnet's multiple comparison test).

lymph node granulomas (*18*, *21*) and in epithelial cells proximal to lung granulomas (*20*). To understand how the RD1-Mmp9 axis mediates granuloma formation, we assessed localization of *mmp9* expression during this process. Fluorescence whole-mount in situ hybridization (FISH) (*1*) revealed RD1-dependent *mmp9* induction in 5-dpi embryos in cells associated with granulomas as well as in distal single cells (Fig. 3A). Multiplex FISH combining the *mmp9* and macrophage-specific *fms* probes, or *mmp9* and neutrophil-specific *mpo* probes (*1*), showed that the distal single cells consisted largely of neutrophils with a minor macrophage contribution (figs. S4 and S5). However, *mmp9* expression by neutrophils and macrophages was unlikely to be relevant for granuloma formation because their *mmp9* expression induced by infection was RD1 independent, and most granulomas contained few, if any, of these cells (Fig. 3B and figs. S4 and S5).

Differential interference contrast (DIC) and confocal microscopy revealed that granuloma-associated *mmp9* expression was localized to epithelial cells proximate to infected macrophages (*22*) (Fig. 3B and movie S1). Expression was restricted to specific epithelial cell types: Epidermal cells adjacent to the granuloma expressed *mmp9*, whereas immediately overlying peridermal cells did not (*22*) (movie S1). Epidermal cell-specific expression was highlighted in granulomas forming in muscle where *mmp9* was expressed not by the immediately surrounding myocytes but by their closest epidermal neighbors (Fig. 3C and movie S2). Every granuloma analyzed had proximate *mmp9*-expressing epithelial cells (n = 35 granulomas in 9 fish), including the smallest identifiable macrophage aggregates (fig. S6 and movie S3). Thus Mmp9 induction is critical for granuloma formation from the very earliest stages and probably in later stages as well, given RD1's continued influence on granuloma structure in chronic tuberculous infection (*5*, *23*).

Bacteria residing in macrophages could induce epithelial cell *mmp9* in two ways: (i) RD1 might induce macrophage signals such as secreted cytokines (*24*, *25*) that in turn elicit *mmp9* secretion by epithelial cells, or (ii) bacteria (*26*, *27*) or bacterial products (*28*) released from macrophages might interact directly with epithelial cells. To distinguish between these mechanisms, we assessed *mmp9* induction in *pu.1* morphants that lack macrophages and in which infection results in extracellular mycobacterial growth (*1*). *pu.1* morphants exhibited RD1-dependent *mmp9* induction, suggesting that bacteria or their products interact directly with epithelial cells to induce

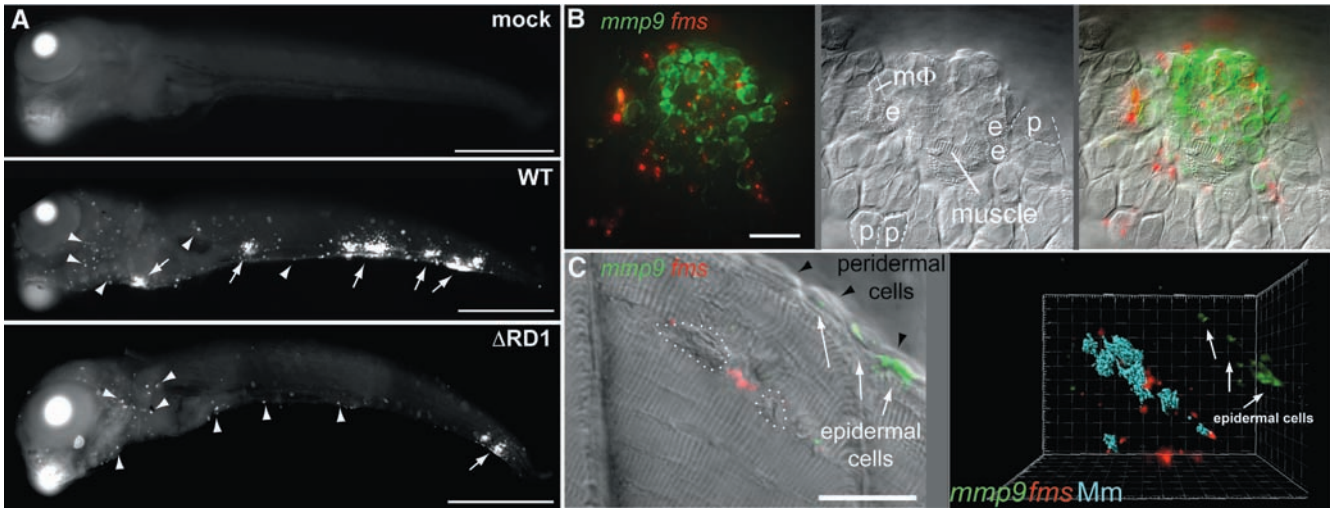

Fig. 3. *mmp9* is selectively induced in epithelial cells neighboring infected macrophages. (**A**) *mmp9* FISH images of embryos 5 days after mock infection or infection with 78 CFU of WT or 130 CFU of ΔRD1. Arrows, *mmp9* expression corresponding to granulomas; arrowheads, single *mmp9*-expressing cells. Scale bars, 400μm. (**B** and **C**) Images of WT granulomas after dual *mmp9* and *fms* FISH. (B) Fluorescence (left), DIC (middle), and overlay (right) images. e, epidermal cell; p, peridermal cell; MΦ, macrophage. Scale bar, 20 μm. Also see movie S1. (C) Fluorescence and DIC overlay of nascent WT muscle granuloma (left). Dotted white circles outline bacterial clusters discerned by DIC microscopy. Fluorescence data have been deconvolved. Right panel represents three-dimensional reconstruction from fluorescence image of the same lesion with bacterial locations pseudocolored blue, showing complete absence of *mmp9* expression in adjacent muscle, and strong *mmp9* expression in nearest neighboring epidermal cells. Scale bar, 20 μm. Also see movie S2.

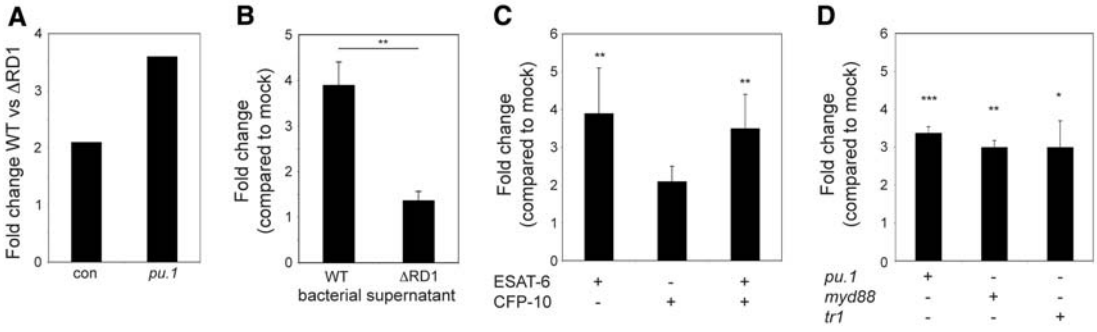

Fig. 4. Mycobacterial ESAT-6 is sufficient to induce *mmp9* in epithelial cells independent of Myd88 and TNF signaling. (**A** to **D**) Relative *mmp9* expression analyzed by real-time quantitative reverse transcriptase–polymerase chain reaction of (A) con or *pu.1* morphant embryos 3 dpi with 84 WT or 126 ΔRD1 (represents one biological replicate), or (B) 34-hpf (hours post fertilization) embryos 4 hours after injection with WT or ΔRD1 bacterial supernatant. Bars represent the means ± SEM of three biological replicates. (C) Thirty-four–hpf con embryos 4 hours after injection with 4.8×10^{-17} mol of purified ESAT-6 or CFP-10, or 4.9×10^{-17} mol of ESAT-6 plus 5.0×10^{-17} mol of CFP-10. Bars represent the means (± SEM) of five biological replicates. (D) Thirty-four–hpf con embryos, *myd88* morphants, or *tr1* morphants 4 hours after injection with 5.7×10^{-17} mol of purified ESAT-6. Bars represent the means ± SEM of four biological replicates (*pu.1* morphant), or three biological replicates (*myd88* and *tr1* morphants).

mmp9 by a macrophage-independent mechanism (Fig. 4A).

The observation that uninfected epithelial cell *mmp9* induction can occur distant from infection foci (Fig. 3C and movie S3) implicated an RD1-dependent secreted determinant rather than direct bacterial contact with epithelial cells. Indeed, injection of WT but not ΔRD1 bacterial supernatants rapidly induced *mmp9* expression (Fig. 4B). The ESX-1 secretion system secretes five proteins that are all mutually codependent for secretion, so distinguishing their individual roles in virulence has been difficult (*14*, *15*). We pursued ESAT-6 as the lead candidate for inducing *mmp9* for two reasons: ESAT-6 mediates virulence independent of secretion (*15*), and its pore-forming activity (*29*, *30*) could allow it direct access to epithelial cells. Injection of 4.8×10^{-17} mol of purified ESAT-6 was sufficient to induce *mmp9* within 4 hours (Fig. 4C). In contrast, 5.0×10^{-17} mol of 10-kD culture filtrate protein (CFP-10), thought to bind ESAT-6 and serve as its chaperone (*15*), failed to induce *mmp9* significantly (Fig. 4C). Moreover, coinjection of CFP-10 and ESAT-6 did not augment the induction observed with ESAT-6 alone, confirming an ESAT-6–specific effect (Fig. 4C). Finally, similar to RD1-competent bacteria (Fig. 4A), ESAT-6 induced *mmp9* in *pu.1* morphants (Fig. 4D), consistent with a direct interaction with epithelial cells. We next asked if epithelial cell *mmp9* induction was dependent on MyD88 and TNF (tumor necrosis factor) signaling, as each can enhance mycobacterial induction of *mmp9* in cultured cells under certain conditions (*19*, *20*). ESAT-6 induced *mmp9* in *myd88* and *tnf-receptor 1* (*tr1*) morphants (Fig. 4D), suggesting a previously unknown pathway for this epithelial cell–specific interaction. Moreover, TNF-independent induction of *mmp9* is consistent with the finding that TNF does not mediate granuloma formation either in the presence or absence of bacterial RD1 (*13*).

Thus, ESAT-6 functions in virulence by promoting granuloma formation via interaction with epithelial cells, previously regarded as bystanders in the pathogenesis of tuberculosis (fig. S7). The cooption of epithelial cells may offer mycobacteria a means of amplifying MMP9 secretion in the vicinity of a single infected macrophage to establish the granuloma niche. In addition, the differential induction of inflammatory programs in macrophages and epithelial cells may generate a hospitable growth niche in macrophages while harnessing epithelial cells to facilitate the chemotaxis of additional macrophages for niche expansion (*6*) (fig. S7). Our work provides a mechanistic explanation for the implication of MMP9 in human susceptibility to tuberculosis (*9*, *11*, *12*) and suggests targeted inhibition of its expression as a host-directed antituberculous therapy. Because increased MMP9 is detrimental in both tuberculosis and a variety of noninfectious inflammatory conditions (*7*), interception of this pathway may have broad utility in treating a variety of inflammatory conditions in addition to tuberculosis.

References and Notes

1. H. Clay *et al.*, *Cell Host Microbe* **2**, 29 (2007).
2. A. J. Wolf *et al.*, *J. Immunol.* **179**, 2509 (2007).
3. D. O. Adams, *Am. J. Pathol.* **84**, 164 (1976).
4. T. Ulrichs, S. H. Kaufmann, *J. Pathol.* **208**, 261 (2006).
5. H. E. Volkman *et al.*, *PLoS Biol.* **2**, e367 (2004).
6. J. M. Davis, L. Ramakrishnan, *Cell* **136**, 37 (2009).
7. P. E. Van den Steen *et al.*, *Crit. Rev. Biochem. Mol. Biol.* **37**, 375 (2002).
8. K. J. Greenlee, Z. Werb, F. Kheradmand, *Physiol. Rev.* **87**, 69 (2007).
9. N. M. Price *et al.*, *J. Immunol.* **166**, 4223 (2001).
10. J. L. Taylor *et al.*, *Infect. Immun.* **74**, 6135 (2006).
11. K. J. Park *et al.*, *Respiration* **72**, 166 (2005).
12. P. Sheen *et al.*, *Eur. Respir. J.* **33**, 134 (2009).
13. H. Clay, H. E. Volkman, L. Ramakrishnan, *Immunity* **29**, 283 (2008).
14. P. A. DiGiuseppe Champion, J. S. Cox, *Cell. Microbiol.* **9**, 1376 (2007).
15. R. Simeone, D. Bottai, R. Brosch, *Curr. Opin. Microbiol.* **12**, 4 (2009).
16. S. C. Derrick, S. L. Morris, *Cell. Microbiol.* **9**, 1547 (2007).
17. J. C. Chang *et al.*, *Thorax* **51**, 306 (1996).
18. N. M. Price, R. H. Gilman, J. Uddin, S. Recavarren, J. S. Friedland, *J. Immunol.* **171**, 5579 (2003).
19. S. Shi *et al.*, *J. Exp. Med.* **198**, 987 (2003).
20. P. T. Elkington *et al.*, *Am. J. Respir. Cell Mol. Biol.* **37**, 431–437 (2007).
21. X. W. Zhu, N. M. Price, R. H. Gilman, S. Recarvarren, J. S. Friedland, *J. Infect. Dis.* **196**, 1076 (2007).
22. D. Le Guellec, G. Morvan-Dubois, J. Y. Sire, *Int. J. Dev. Biol.* **48**, 217 (2004).
23. D. R. Sherman *et al.*, *J. Infect. Dis.* **190**, 123 (2004).
24. I. C. Koo *et al.*, *Cell. Microbiol.* **10**, 1866 (2008).
25. S. A. Stanley, S. Raghavan, W. W. Hwang, J. S. Cox, *Proc. Natl. Acad. Sci. U.S.A.* **100**, 13001 (2003).
26. L. M. Stamm *et al.*, *J. Exp. Med.* **198**, 1361 (2003).
27. M. Hagedorn, K. H. Rohde, D. G. Russell, T. Soldati, *Science* **323**, 1729 (2009).
28. D. G. Russell, *Nat. Rev. Microbiol.* **5**, 39 (2007).
29. T. Hsu *et al.*, *Proc. Natl. Acad. Sci. U.S.A.* **100**, 12420 (2003).
30. M. I. de Jonge *et al.*, *J. Bacteriol.* **189**, 6028 (2007).
31. Materials and methods are available as supporting material on *Science* Online.

32. We thank J. I. Gordon, W. Parks, D. Raible, D. Sherman, K. Urdahl, and P. Elkington for advice and discussion; D. Beery and R. Kim for help with microinjections; and J. Cameron, L. Swaim, and H. Wiedenhoft for fish facility maintenance. We also thank K. Winglee for developing FPC analysis methods, R. Burmeister for graphic design, and D. Tobin, B. Cormack, W. Parks, D. Stetson, R. Berg, and F. Chu for review of the manuscript. This work was supported by the Burroughs Wellcome Fund (L.R.), the Pew Scholars Program (J.F.R.), the NIH (L.R. and J.F.R.), an American Heart Association predoctoral fellowship (H.E.V.), a Pediatric Infectious Diseases Society postdoctoral award, the Children's Health Research Center new investigator award, an NIH diversity supplement (T.C.P.), and a National Defense Science and Engineering predoctoral fellowship (J.M.D.).

Supporting Online Material

www.sciencemag.org/cgi/content/full/science.1179663/DC1
Materials and Methods
Figs. S1 to S7
Tables S1 to S4
References
Movies S1 to S3

24 July 2009; accepted 19 November 2009
Published online 10 December 2009;
10.1126/science.1179663
Include this information when citing this paper.

Evolution of MRSA During Hospital Transmission and Intercontinental Spread

Simon R. Harris,[1]* Edward J. Feil,[2]* Matthew T. G. Holden,[1] Michael A. Quail,[1] Emma K. Nickerson,[3,4] Narisara Chantratita,[3] Susana Gardete,[5,6] Ana Tavares,[5] Nick Day,[3,7] Jodi A. Lindsay,[8] Jonathan D. Edgeworth,[9,10] Hermínia de Lencastre,[5,6] Julian Parkhill,[1] Sharon J. Peacock,[3,4] Stephen D. Bentley[1]†

Current methods for differentiating isolates of predominant lineages of pathogenic bacteria often do not provide sufficient resolution to define precise relationships. Here, we describe a high-throughput genomics approach that provides a high-resolution view of the epidemiology and microevolution of a dominant strain of methicillin-resistant *Staphylococcus aureus* (MRSA). This approach reveals the global geographic structure within the lineage, its intercontinental transmission through four decades, and the potential to trace person-to-person transmission within a hospital environment. The ability to interrogate and resolve bacterial populations is applicable to a range of infectious diseases, as well as microbial ecology.

The development of molecular typing techniques has been instrumental in studying the population structure and evolution of bacterial pathogens. Sequence-based approaches, such as multilocus sequence typing (MLST) (*1*), have resulted in large searchable databases of the most clinically important species. However, MLST defines variation within a very small sample of the genome and cannot distinguish between closely related isolates. Full-genome sequencing provides a complete inventory of microevolutionary changes, but this approach is impractical for large population samples. The use of next-generation sequencing technologies, such as Illumina Genome Analyzer, bridges this gap by mapping genome-wide single-nucleotide poly-